DOI: 10.1002/chem.201000460

Tuning the HOMO Energy Levels of Organic Dyes for Dye-Sensitized Solar Cells Based on Br^-/Br_3^- Electrolytes

Chao Teng,[a] Xichuan Yang,*[a] Shifeng Li,[a] Ming Cheng,[a] Anders Hagfeldt,[a, b]
Li-zhu Wu,[c] and Licheng Sun*[a, d]

Abstract: A series of novel metal-free organic dyes **TC301–TC310** with relatively high HOMO levels were synthesized and applied in dye-sensitized solar cells (DSCs) based on electrolytes that contain Br^-/Br_3^- and I^-/I_3^-. The effects of additive Li^+ ions and the HOMO levels of the dyes have an important influence on properties of the dyes and performance of DSCs. The addition of Li^+ ions in electrolytes can broaden the absorption spectra of the dyes on TiO_2 films and shift both the LUMO levels of the dyes and the conduction band of TiO_2, thus leading to the increase of J_{sc} and the decrease of V_{oc}. Upon using Br^-/Br_3^- instead of I^-/I_3^-, a large increase of V_{oc} is attributed to the enlarged energy difference between the redox potentials of electrolyte and the Fermi level of TiO_2, as well as the suppressed electron recombination. Incident photon to current efficiency (IPCE) action spectra, electrochemical impedance spectra, and nanosecond laser transient absorption reveal that both the electron collection yields and the dye regeneration yields (Φ_r) depend on the potential difference (the driving forces) between the oxidized dyes and the Br^-/Br_3^- redox couple. For the dyes for which the HOMO levels are more positive than the redox potential of Br^-/Br_3^- sufficient driving forces lead to the longer effective electron-diffusion lengths and almost the same efficient dye regenerations, whereas for the dyes for which the HOMO levels are similar to the redox potential of Br^-/Br_3^-, insufficient driving forces lead to shorter effective electron-diffusion lengths and inefficient dye regenerations.

Keywords: bromides · charge transfer · dyes/pigments · energy conversion · sensitizers

Introduction

Dye-sensitized solar cells (DSCs), as a promising technology for low-cost photovoltaics, have attracted much attention in the past two decades owing to their high efficiency of approximately 12% and their high stability under prolonged light and thermal dual stress.[1] A DSC employs a nanocrystalline porous semiconductor metal oxide such as TiO_2 that is sensitized by dye and infiltrated by liquid electrolyte that contains a redox mediator. The dye is excited by solar-light absorption and injects an electron into the conduction band of TiO_2. Thus the oxidized state of the dye is obtained. The oxidized state of the dye receives an electron from a redox mediator in the electrolyte and is regenerated. The common choice of redox mediator for obtaining high solar-cell efficiencies in liquid electrolyte is iodide/triiodide (I^-/I_3^-).[2] The lowest unoccupied molecular orbital (LUMO) level of the dye should be sufficiently more negative than the conduction band of TiO_2 ($E_{cb} = -0.5$ V vs. normal hydrogen electrode (NHE)) for efficient electron injection, and meanwhile the highest occupied molecular orbital (HOMO) level of the dye should be sufficiently more positive than the po-

---

[a] C. Teng, Prof. X. Yang, S. Li, M. Cheng, Prof. A. Hagfeldt,
Prof. L. Sun
State Key Laboratory of Fine Chemicals
DUT-KTH Joint Education
and Research Center on Molecular Devices
Dalian University of Technology (DUT), Dalian (China)
Fax: (+86) 411-837-02185
E-mail: yangxc@dlut.edu.cn

[b] Prof. A. Hagfeldt
School of Chemical Science and Engineering
Center of Molecular Devices, Physical Chemistry
Royal Institute of Technology (KTH), Stockholm (Sweden)

[c] Prof. L.-z. Wu
Key Laboratory of Photochemical Conversion
and Optoelectronic Materials
Technical Institute of Physics and Chemistry
Chinese Academy of Sciences, Beijing (China)

[d] Prof. L. Sun
Department of Chemistry, Organic Chemistry
Royal Institute of Technology(KTH), Stockholm (Sweden)

Supporting information for this article is available on the WWW under http://dx.doi.org/10.1002/chem.201000460.

tential of redox mediator in electrolyte for efficient dye regeneration. Efficient operation of DSC relies on both efficient electron injection and efficient dye regeneration. So far, the most efficient DSCs with record high efficiency of around 12% are based on Ru dye N719 and I^-/I_3^-[3] redox mediator.[4]

Compared to the great efforts spent on the design and synthesis of different dyes, less study has been devoted to the redox mediators. Ferrocene/ferrocenium (Fc/Fc^+) has been tested as a redox mediator, but it yielded a low open-circuit voltage (V_{oc}) and a small short-circuit photocurrent density (J_{sc}).[5] Co^{II} complexes showed an impressive efficiency of 8% at low light intensity but their performance drops remarkably under full-sun illumination.[6] Stable organic radical 2,2,6,6-tetramethyl-1-piperidinyloxy (TEMPO) has been shown to give a V_{oc} of 0.86 V (vs. NHE) and an efficiency of 5.4% under simulated AM 1.5 full sunlight (100 mW cm^{-2}) irradiation.[7]

The theoretical maximum of V_{oc} is a crucial parameter for DSC and is determined by the energy difference between the potential of redox mediator in electrolyte and the Fermi level of TiO_2. Therefore one possible method to increase V_{oc} is to find a new redox mediator with a more positive potential than $E(I^-/I_3^-)$.[8] Br^-/Br_3^- is a promising candidate because of its much more positive redox potential (up to 1.1 V vs. NHE) than $E(I^-/I_3^-)$ (approximately 0.4 V).[9] Recently, we published the synthesis and characterization of two novel carbazole dyes (**TC301** and **TC306**, Scheme 1) for DSCs with high V_{oc} up to 1 V and good solar-energy conversion efficiencies based on electrolytes that contain Br^-/Br_3^-.[10] To fine-tune the HOMO level of the dye and to gain further insight into the relationship between the structure of the dye and the performance of DSC based on the Br^-/Br_3^- redox couple, here we report the design, synthesis, and characterization of a series of novel metal-free organic dyes (**TC301–TC310**, the detailed structures are shown in Scheme 1) in which triphenylamine (**TC301–TC306**) or carbazole derivatives (**TC307–TC310**) were used as electron donors, and cyanoacrylic acid as an electron-accepting/anchoring moiety. The performance of solar cells based on these new organic dyes and the redox couple Br^-/Br_3^- in comparison with I^-/I_3^- has been investigated by electrochemistry, impedance spectra, and transient absorption spectroscopy, as well as time-dependent density functional theory (TD-DFT) calculations.

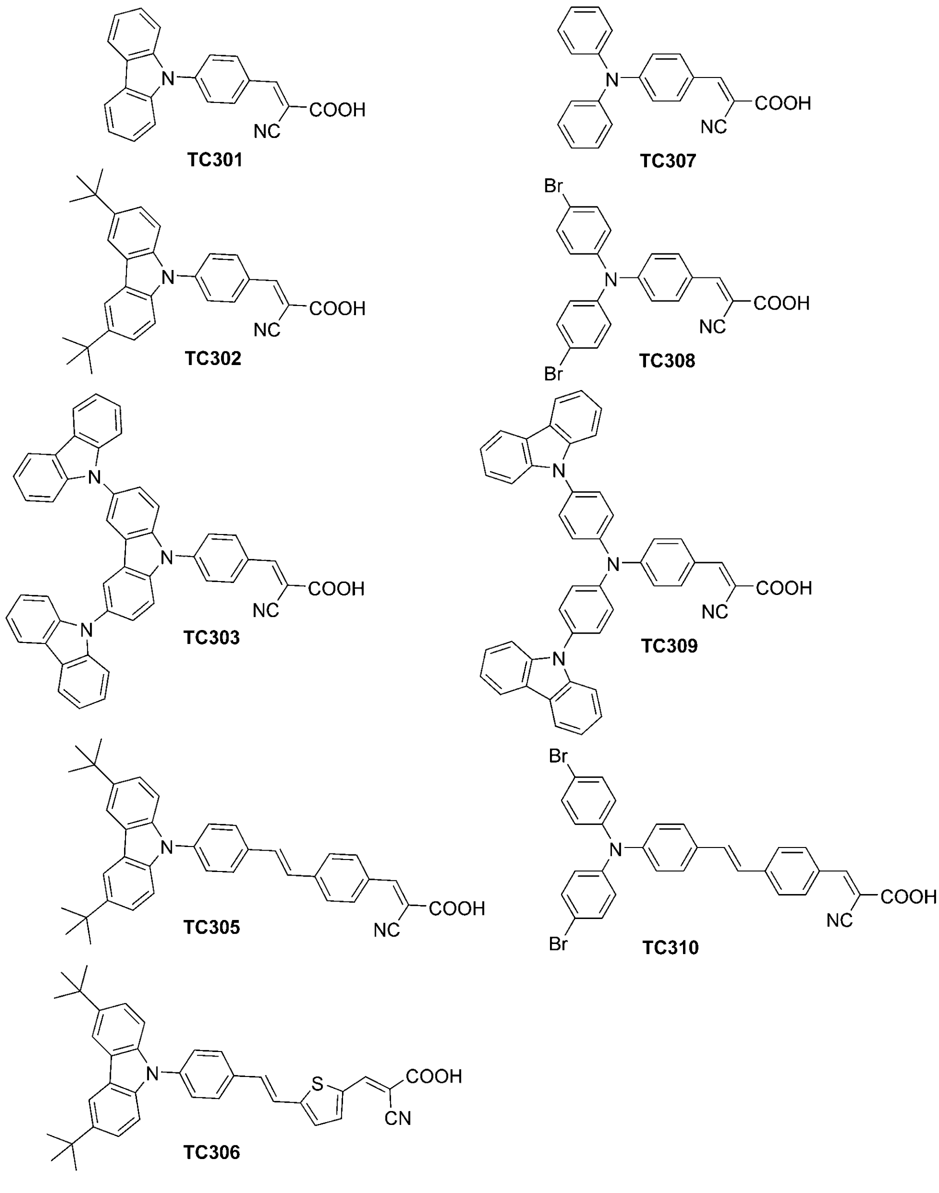

Scheme 1. Molecular structures of a series of metal-free organic dyes **TC301–TC310** for application in DSCs with Br^-/Br_3^- as redox couple.

Results and Discussion

Photophysical properties: Absorption spectra of solutions of **TC301–TC310** in CH_3CN are displayed in Figure 1, and the corresponding data are presented in Table 1. All the dyes

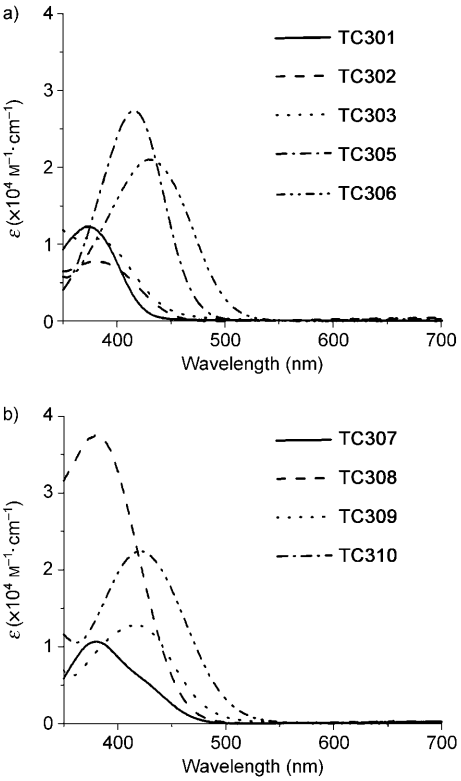

Figure 1. Absorption spectra of solutions of the dyes in CH_3CN (2×10^{-5} M): a) **TC301–TC306** with triphenylamine derivatives as electron donors; b) **TC307–TC310** with carbazole derivatives as electron donors.

Table 1. Absorption, emission, and electrochemical properties of **TC301–TC310**.

Dye	λ_{max}^{abs} [a] [nm]	ε [$M^{-1}cm^{-1}$]	λ_{max}^{em} [b] [nm]	E_{ox}[c] [V vs. NHE]	λ_{max} on TiO_2 [nm]	$E_{0\text{-}0}$ abs/em[f] [V]	$E_{ox}-E_{0\text{-}0}$ [V vs. NHE]
TC301	374	12300	527	1.59	384[d]	2.82	−1.23
					392[e]	2.68	−1.09
TC302	381	7800	551	1.46	391[d]	2.71	−1.35
					407[e]	2.58	−1.12
TC303	378	10800	423	1.45	387[d]	2.83	−1.38
					398[e]	2.70	−1.25
TC305	416	27400	543	1.48	400[d]	2.63	−1.15
					407[e]	2.51	−1.03
TC306	429	21000	553	1.38	411[d]	2.44	−1.06
					425[e]	2.34	−0.96
TC307	381	10700	515	1.33	405[d]	2.63	−1.30
					412[e]	2.48	−1.15
TC308	379	37300	560	1.43	383[d]	2.66	−1.23
					389[e]	2.54	−1.11
TC309	418	12800	557	1.24	407[d]	2.54	−1.30
					414[e]	2.43	−1.19
TC310	421	22400	559	1.12	400[d]	2.50	−1.38
					407[e]	2.40	−1.28

[a] Absorption in CH_3CN (2×10^{-5} M) at RT. [b] Emission spectrum in CH_3CN (2×10^{-5} M) at RT. [c] The oxidation potential of the dyes was measured in DMF with $TBAPF_6$ (0.1 M) as electrolyte (working electrode: glassy carbon; reference electrode: Ag/Ag^+; calibrated with Fc/Fc^+ as an internal reference and converted to NHE by addition of 630 mV;[16] counterelectrode: Pt). [d] Absorption of dye loaded on TiO_2 film immersed in CH_3CN without electrolyte. [e] Absorption of dye loaded on TiO_2 film immersed in CH_3CN with 0.8 M LiBr in electrolyte. [f] $E_{0\text{-}0}$ was determined by the onset wavelength of the corresponding absorption spectrum on TiO_2 films.

with a strong absorption maximum (λ_{max}) located in the spectral range of 370–430 nm, which corresponds to HOMO to LUMO transitions, are observed.[11] The values of molar extinction coefficient (ε) at λ_{max} are in the range of 1.0×10^4–3.7×10^4 $M^{-1}cm^{-1}$. The absorption spectrum of **TC301** shows a λ_{max} at 374 nm ($\varepsilon = 12300\ M^{-1}cm^{-1}$; Figure 1a). Compared to **TC301**, the absorption spectra of **TC302** and **TC303** are slightly redshifted because the introduction of *tert*-butyl or carbazolyl groups enhances the electron-donating abilities of an electron donor. Enlarging the π conjugation of **TC301** to give **TC305** and **TC306** caused a further redshift to 416 nm ($\varepsilon = 27400\ M^{-1}cm^{-1}$) and 429 nm ($\varepsilon = 21000\ M^{-1}cm^{-1}$), respectively. Compared to **TC307**, the absorption spectrum of **TC308** changes only little (Figure 1b), thereby revealing that the introduction of a bromo group into the electron-donor part has almost no influence on the absorption spectrum of the dye. The redshifted absorption spectra of **TC309** and **TC310** relative to that of **TC307** are also caused by the enhancement of the electron donor and the increase in π conjugation. We can see from Figure 2 that a blueshifting effect of the absorption spectra of the dyes **TC301**, **TC306**, and **TC310** was observed with an increase in the polarity of the solvent from CH_2Cl_2 to CH_3CN.[12]

When the dyes were attached onto TiO_2 films, the absorption spectra may shift to the blue or red region compared to that in solutions because of the interaction between the dyes and the semiconductor surface. In general, the larger shift of the absorption spectra of the dyes on TiO_2 films compared with that in solutions could indicate a higher tendency to form aggregation on TiO_2 film.[13] The idea of suppressing the dye aggregation on TiO_2 film and anchoring the dye monolayer onto the TiO_2 surface has been considered to give higher efficiency of a DSC. We can see from Figures 1 and 2 and Table 1 that all the absorption spectra of **TC301–TC310** on TiO_2 films only shifted slightly in comparison to those in CH_3CN solutions. This indicates that **TC301–TC310** have less of a tendency to form aggregation on TiO_2 films and can likewise achieve higher efficiencies of DSCs.

Electrochemical properties: To fine-tune the HOMO levels of the dyes, we changed the structures of the dyes by introduction of different electron donors and linkers. We can see from Table 1 that the first oxidation potentials (E_{ox}) that correspond to the HOMO levels of dyes changed negatively upon enhancing the electron donor and increasing π conjugation. The HOMO level of **T310** is almost similar to $E(Br^-/Br_3^-)$,

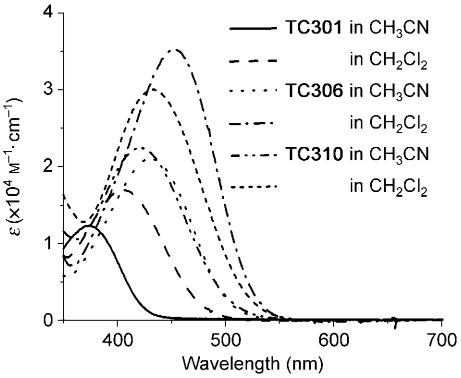

Figure 2. Absorption spectra of solutions of the selected dyes in CH_3CN (2×10^{-5} M) compared to those in CH_2Cl_2 (2×10^{-5} M).

whereas the HOMO levels of **TC301–TC309** are all more positive than $E(Br^-/Br_3^-)$. The different HOMO levels of the dyes could help us scrutinize the relationship between the structure of the dye and the performance of DSC based on electrolytes that contain Br^-/Br_3^-.

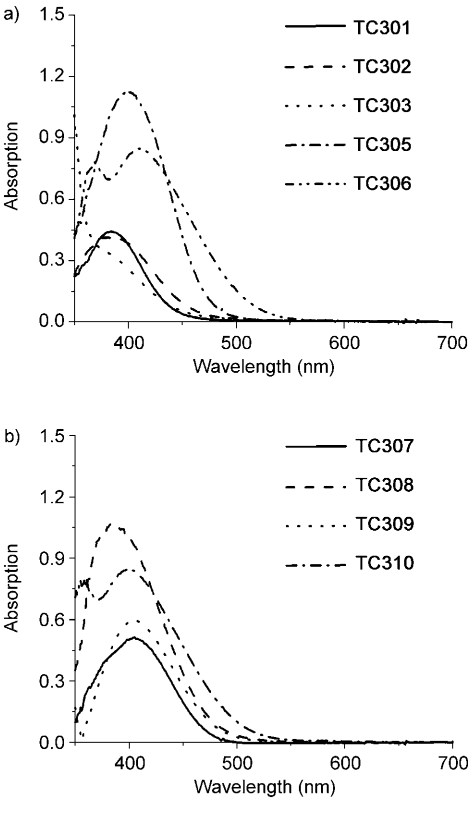

Figure 3. Absorption spectra of the dyes on TiO_2 films: a) **TC301–TC306** with triphenylamine as electron donors; b) **TC307–TC310** with carbazole as electron donors.

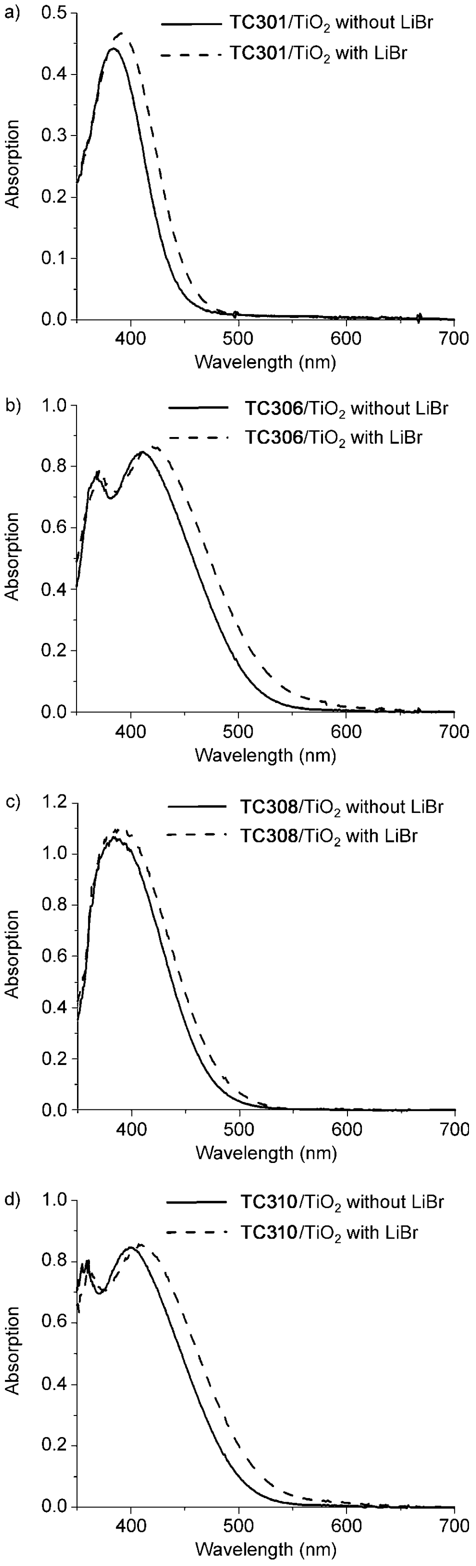

Figure 4. Absorption spectra of the selected dyes attached on TiO_2 films immersed in CH_3CN with 0.8 M LiBr and without electrolyte. a) **TC301** on TiO_2 films; b) **TC306** on TiO_2 films; c) **TC308** on TiO_2 films; and d) **TC310** on TiO_2 films.

The LUMO level of the dye was calculated by $E_{ox}-E_{0-0}$, in which E_{0-0} was determined by the onset wavelength of the corresponding absorption spectrum on TiO_2 films (Figure 3). It is evident that the values of $E_{ox}-E_{0-0}$ are more negative than E_{cb}, thus all the dyes can complete the process of electron injection into the conduction band (cb) of TiO_2

Table 2. Frontier molecular orbitals of the HOMO and LUMO calculated with DFT at the B3LYP/6-31+G(d) level of the selected dyes.

Dye	HOMO	LUMO
TC301	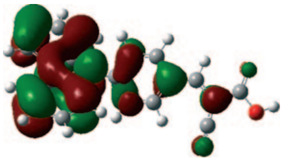	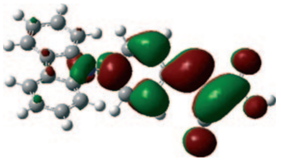
TC306	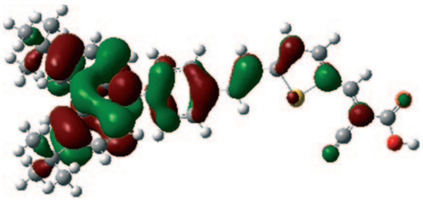	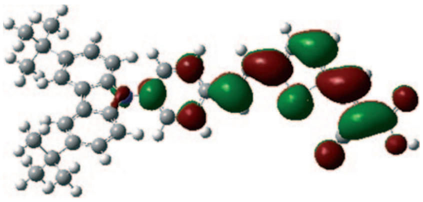
TC308	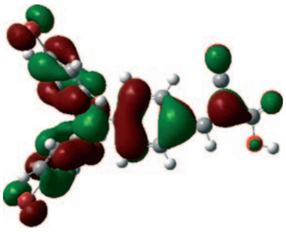	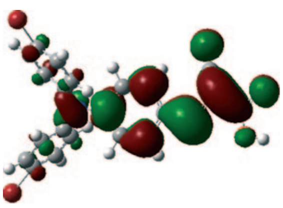
TC310		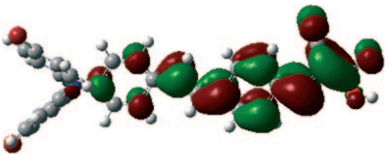

to form the oxidized dyes. Noticeably, the relatively large energy gaps between the LUMO levels of the dyes and the conduction band of TiO_2 allow for the addition of tributyl phosphate (TBP) into the electrolyte, which can shift the conduction band of TiO_2 negatively about 0.3 V and consequently improve V_{oc} and total solar-energy-to-electricity conversion efficiency.[14]

Li^+-ion effects on photoelectrochemical properties: With a view towards practical development of high-performance DSCs, the effects of additives to electrolyte have been extensively investigated. It is well known that the adsorption/intercalation of potential determining cations such as Li^+ ions into the porous TiO_2 electrode can broaden the absorption of the dye on TiO_2.[15] Figure 4 shows the absorption spectra of the selected dyes on TiO_2 films immersed in CH_3CN with 0.8 M LiBr as additive and without electrolyte. The various solvents used here were exchanged between measurements while the samples were maintained in a fixed position in the measurement cell. Thus, the changes of absorbance observed in different solvents most likely corresponded to changes in the absorption coefficient of the dyes on the TiO_2 surface. We can see from Figure 4 and Table 1 that the absorption spectra of **TC301–TC310** on TiO_2 films immersed in CH_3CN solutions with 0.8 M LiBr are all redshifted about 10 nm relative to that without electrolyte. Redshift of the absorption on TiO_2 films led to the E_{0-0} change, thus the LUMO levels of **TC301–TC310** shifted positively about 100 mV in the presence of 0.8 M LiBr.

DFT study: To gain insight into the geometrical electronic structures of the dyes, we performed DFT calculations on the dyes using the Gaussian 03 program package. In particular, we used B3LYP as exchange-correlation functional and 6-31+G (d) as the basis set.[17] At the ground state (HOMO) of the dyes, electrons are homogeneously distributed on electron-donor part. At the excited state (LUMO), intramolecular charge-transfer occurs, thereby resulting in the electron movement to the electron-acceptor part (cyanoacrylic acid). The frontier molecular orbital of the dyes reveals that HOMO–LUMO excitation moves the electron-density distribution from the electron-donor moiety to the electron-acceptor moiety by means of different π conjugation. Thus the change in electron distribution induced by photoexcitation results in an efficient charge separation (Table 2).

Photocurrent–photovoltage characteristics: To compare the performance of DSCs based on electrolytes that contain Br^-/Br_3^- and those which contain I^-/I_3^- and the effects of the addition of Li^+ ions, three kinds of devices (devices A, B, and C) were constructed. Devices A are DSCs based on Br^-/Br_3^- and contain 0.9 M 1,2-dimethyl-3-butylimidazolium bromide (DMBIBr), 0.08 M Br_2, and 0.5 M TBP electrolyte in dry CH_3CN. Devices B are DSCs also based on Br^-/Br_3^- and contain 0.9 M DMBIBr, 0.8 M LiBr, 0.08 M Br_2, and 0.5 M TBP electrolyte in dry CH_3CN. As reference, devices C are DSCs based on I^-/I_3^- and contain 0.6 M 1, 2-dimethyl-3-propylimidazolium iodide (DMPII), 0.06 M LiI, 0.04 M I_2, and 0.4 M TBP electrolyte in dry CH_3CN. Figure 5 shows the photocurrent–photovoltage characteristics for **TC301–TC310** and for devices A, B, and C under simulated AM 1.5 irradiation (100 mW cm^{-2}); the detailed photovoltaic parameters are listed in Table 3. A DSC that consisted of Br^-/Br_3^- and **TC301** accomplished a very high open-circuit voltage (up to 1.156 V) with a good solar-energy-conversion efficiency of 3.68 % (Figure 5a). For the **TC306**-based DSC, a high open-circuit voltage (up to 0.939 V) with a considerably good solar-energy-conversion efficiency of 5.22 % was also achieved with an electrolyte that contained Br^-/Br_3^- (Figure 5c). These results suggest that Br^-/Br_3^- could be a promising alternative to I^-/I_3^- for DSCs with dyes for which the HOMO levels are more positive than $E(Br^-/Br_3^-)$.

When replacing I^-/I_3^- with Br^-/Br_3^- in **TC301–TC310**-based DSCs, both devices A and B yielded a significant increase in V_{oc} than devices C. This was attributed to the enlarged energy difference between the redox potential of the electrolyte and the Fermi level of TiO_2. The V_{oc} of devices B are slightly lower than those of devices A due to the positive shift of the conduction band of TiO_2 in the presence of Li^+ ions.[8b,18] And the higher J_{sc} in devices B compared with devices A was attributed to the broader absorption of the dyes on TiO_2 films in the presence of Li^+ ions. We can see from Figure 5 and Table 3 that upon using Br^-/Br_3^- instead of I^-/I_3^-, DSCs sensitized by **TC301–TC308** produced much higher V_{oc} and led to much higher η; the DSC sensitized by **TC309** produced much higher V_{oc} and almost the same η, but the DSC sensitized by **TC310** produced much lower η along with much higher V_{oc} because of the large decrease in J_{sc}. One of the main reasons for such differences in solar-cell performance may be the different energy gaps between the HOMO levels of the dyes and $E(Br^-/Br_3^-)$, which lead to the different driving forces for dye regeneration.

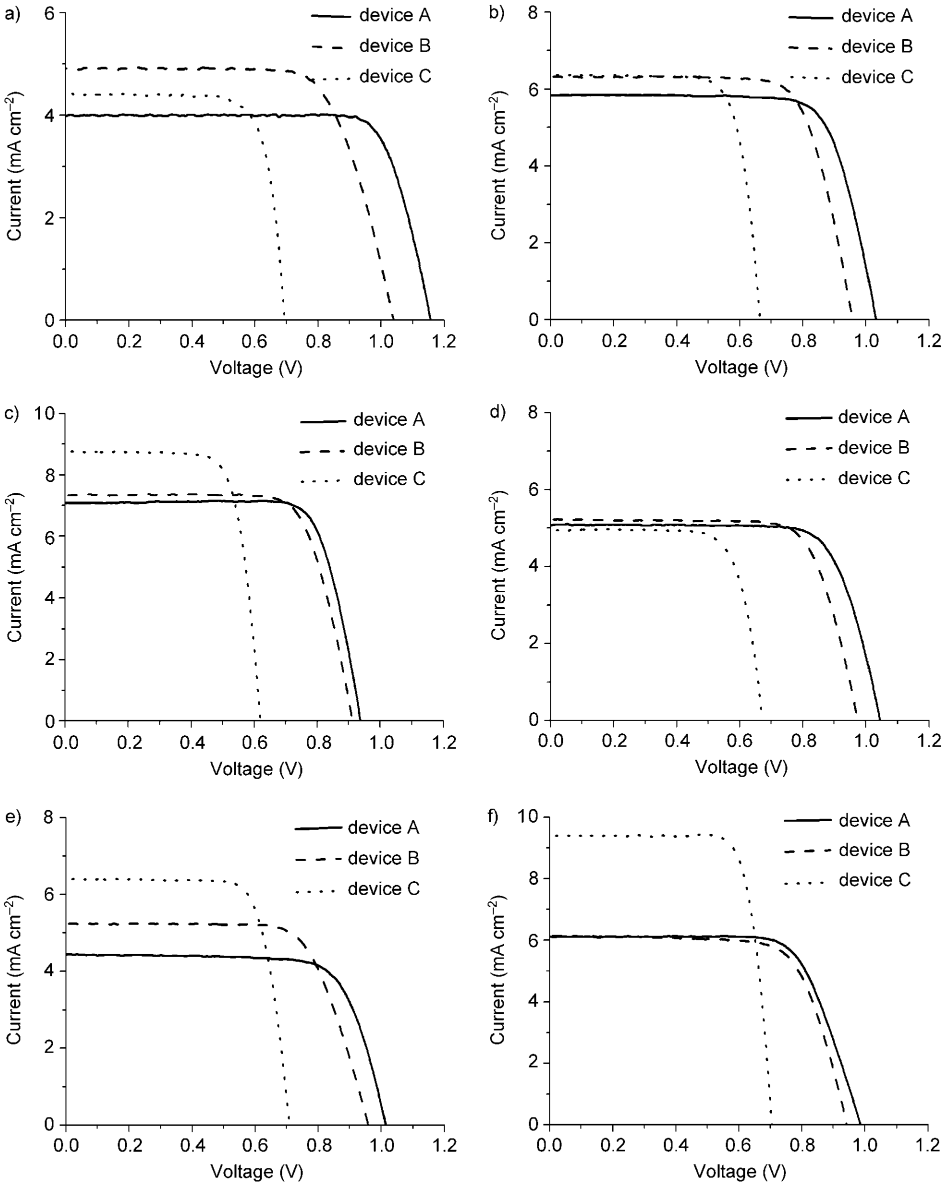

Figure 5. Photocurrent density versus voltage curves for DSC sensitized by the selected dyes with different electrolytes: device A based on 0.9 M DMBIBr, 0.08 M Br_2, and 0.5 M TBP electrolyte in dry CH_3CN; device B based on 0.9 M DMBIBr, 0.8 M LiBr, 0.08 M Br_2, and 0.5 M TBP electrolyte in dry CH_3CN; and device C based on 0.6 M DMPII, 0.06 M LiI, 0.04 M I_2, and 0.4 M TBP electrolyte in dry CH_3CN. a) DSC sensitized by **TC301**, b) DSC sensitized by **TC305**, c) DSC sensitized by **TC306**, d) DSC sensitized by **TC308**, e) DSC sensitized by **TC309**, and f) DSC sensitized by **TC310**.

Incident photon-to-current conversion efficiency (IPCE) action spectra: For DSCs sensitized by **TC301–TC310**, the IPCE plateaus are all between 360 and 500 nm (Figure 6), and IPCE maxima are above 70 % upon using electrolytes that contain Br^-/Br_3^- or I^-/I_3^-. Considering the light absorption and scattering loss by the conducting glass, the maxima efficiencies for absorbed photon-to-collected-electron conversion efficiencies (APCEs) are very high, thus suggesting very high charge-collection yields. Because of the lower absorption of bromine relative to that of iodine below 400 nm (Figure 7), devices A and B produced larger IPCE values compared to devices C in this spectral region, except for DSC sensitized by **TC310**. And we find that IPCE maxima produced by electrolytes that contain Br^-/Br_3^- are very similar to those produced by those that contain I^-/I_3^-, also except for DSC sensitized by **TC310**. Assuming the electron injection is independent of the redox mediator,[19] the similar IPCE maxima of DSC sensitized by **TC301–TC309** may be due to the similar dye-regeneration efficiencies upon using Br^-/Br_3^- and I^-/I_3^-. For DSC sensitized by **TC310**, the much smaller IPCE maxima of DSC based on Br^-/Br_3^- may be due to much less dye-regeneration efficiency than that based on I^-/I_3^-.

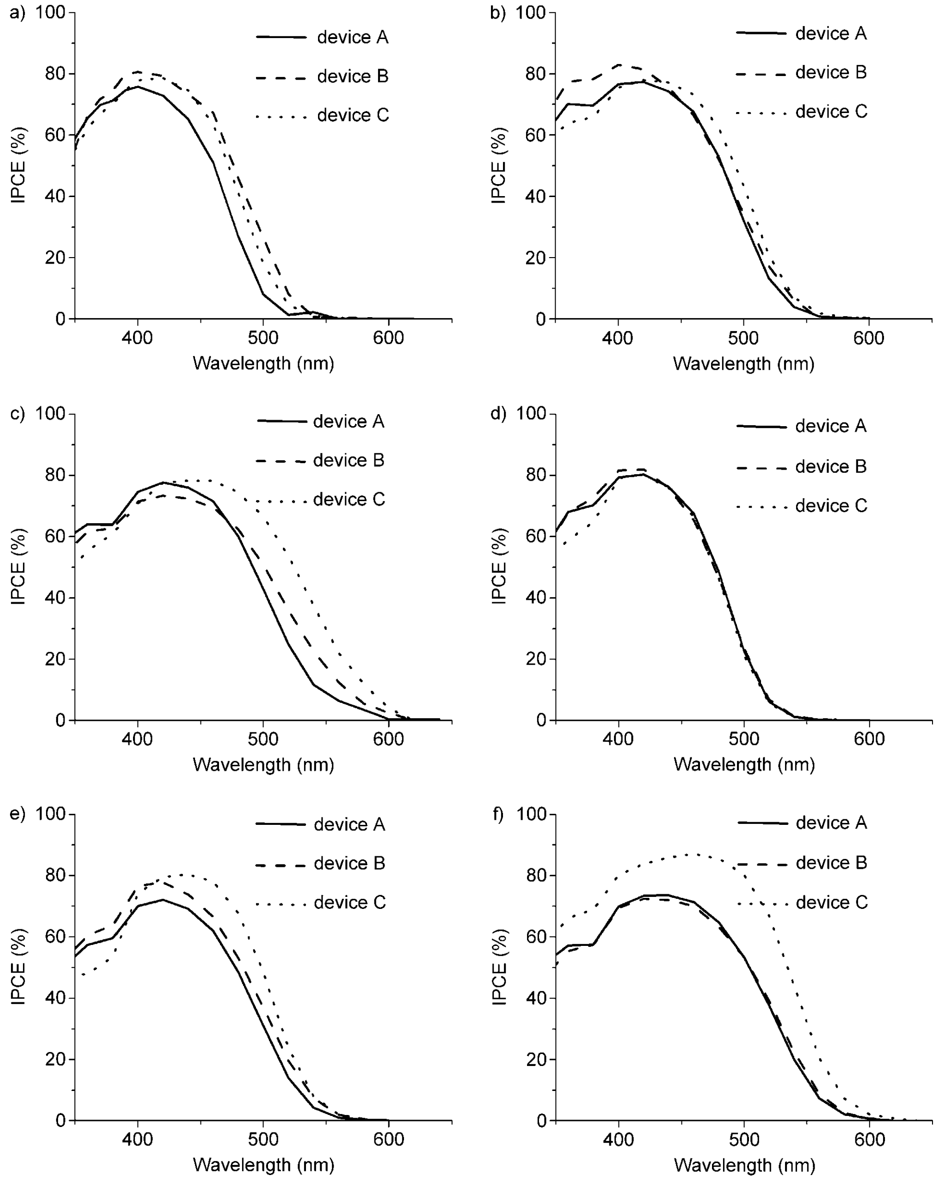

Figure 6. IPCE action spectra for dye-sensitized solar cells sensitized by the dyes **TC301–309** with different electrolytes: device A based on 0.9 M DMBIBr, 0.08 M Br_2, and 0.5 M TBP electrolyte in dry CH_3CN; device B based on 0.9 M DMBIBr, 0.8 M LiBr, 0.08 M Br_2, and 0.5 M TBP electrolyte in dry CH_3CN; and device C based on 0.6 M DMPII, 0.06 M LiI, 0.04 M I_2, and 0.4 M TBP electrolyte in dry CH_3CN. a) DSC sensitized by **TC301**, b) DSC sensitized by **TC305**, c) DSC sensitized by **TC306**, d) DSC sensitized by **TC308**, e) DSC sensitized by **TC309**, and f) DSC sensitized by **TC310**.

Electrochemical impedance spectroscopy: We can see from Figure 5 and Table 3 that upon using Br^-/Br_3^- instead of I^-/I_3^-, distinctive solar-energy-conversion efficiencies were obtained by DSCs sensitized by **TC308** and **TC310**. To gain further insight into the interfacial charge-transfer processes in DSCs based on electrolytes that contain I^-/I_3^- or Br^-/Br_3^-, we chose **TC308** and **TC310** as subjects for electrochemical impedance spectra (EIS) analysis. The Nyquist plots and Bode phase plots are shown in Figure 8, and the detailed parameters are shown in Table 4. The small semicircle in the Nyquist plots, which corresponds to the high-frequency peaks in the Bode phase plots, represents the electron transfer from Pt counterelectrode to the oxidized species in the electrolyte, that is, the reduction of the oxidized species to the reduced species. The large semicircle in the Nyquist plots, which corresponds to the midfrequency peaks in the Bode phase plots, represents the charge recombination that arises from electrons in TiO_2 film recombining with I_3^- ion in the electrolyte.

From Figure 8 we find that the high-frequency peaks in the Bode phase plots also shifted to lower frequency upon using Br^-/Br_3^- instead of I^-/I_3^-. Correspondingly, in the Nyquist plots, the small semicircle showed a larger resistance for Br^-/Br_3^- than for I^-/I_3^-. This means that the reduction of bromine is slower than that of iodine at the Pt counterelectrode.

By fitting the EIS curves, we can obtain some important parameters for the devices. One is the electron lifetime (τ), which could be extracted from the angular frequency (ω_{min}) at the midfrequency peak in the Bode phase plot by using $\tau = 1/\omega_{min}$ and expresses for electron recombination in TiO_2 films.[20] R_{ct} and R_t represent charge-transfer resistance at the dye/TiO_2/electrolyte interface related to electron recombination and the electron-transport resistance in TiO_2 film, respectively. Another important parameter is the effective electron-diffusion length (L_n) in TiO_2 films, which could be extracted by using $L_n = L(R_{ct}/R_t)^{1/2}$ (L is the thickness of TiO_2 film);[21] it reflects the competition between charge collection and recombination.

The electron lifetimes (τ) and the charge-transfer resistances (R_{ct}) of devices A and B are much larger than those of devices C. The significant increase in τ and R_{ct} means that the electron recombination that arises from electrons in TiO_2 film with I_3^- ion in electrolyte is suppressed upon replacing I^-/I_3^- with Br^-/Br_3^-. Thus we can conclude that significant increase in V_{oc} by using Br^-/Br_3^--based electrolytes instead of those based on I^-/I_3^- were attributed to not only the enlarged energy difference between the redox potential

Table 3. Photovoltaic performance of DSC sensitized by **TC301–TC310** in different electrolytes.

Dye	Device[a]	J_{sc} [mA cm^{-2}]	V_{oc} [V]	ff [%]	η [%]
TC301	A	4.00	1.156	0.796	3.68
	B	4.93	1.041	0.713	3.66
	C	4.42	0.696	0.767	2.36
TC302	A	4.71	1.091	0.788	4.05
	B	5.27	1.009	0.749	3.98
	C	4.64	0.721	0.778	2.60
TC303	A	3.88	1.077	0.784	3.28
	B	4.27	0.969	0.756	3.13
	C	4.13	0.692	0.775	2.21
TC305	A	5.83	1.033	0.766	4.61
	B	6.31	0.959	0.751	4.54
	C	6.35	0.665	0.764	3.23
TC306	A	7.12	0.939	0.781	5.22
	B	7.36	0.915	0.752	5.07
	C	8.76	0.621	0.754	4.10
TC307	A	3.73	0.946	0.750	2.65
	B	4.02	0.881	0.774	2.74
	C	4.90	0.620	0.744	2.26
TC308	A	5.08	1.045	0.765	4.06
	B	5.19	0.976	0.760	3.85
	C	4.95	0.673	0.746	2.48
TC309	A	4.41	1.015	0.755	3.38
	B	5.23	0.960	0.723	3.63
	C	6.39	0.710	0.764	3.47
TC310	A	6.12	0.988	0.728	4.40
	B	6.06	0.945	0.735	4.21
	C	9.39	0.706	0.791	5.24

[a] Device A is based on 0.9 M DMBIBr, 0.08 M Br_2, and 0.5 M TBP electrolyte in dry CH_3CN. Device B is based on 0.9 M DMBIBr, 0.8 M LiBr, 0.08 M Br_2, and 0.5 M TBP electrolyte in dry CH_3CN. Device C is based on 0.6 M DMPII, 0.06 M LiI, 0.04 M I_2, and 0.4 M TBP electrolyte in dry CH_3CN.

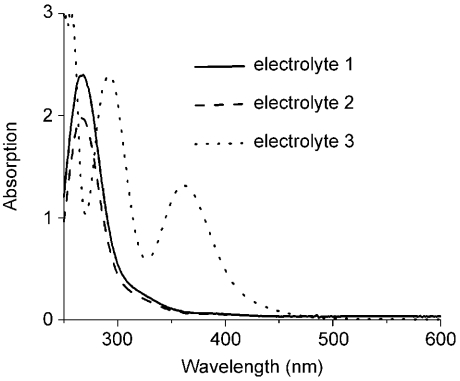

Figure 7. Absorption spectra of the different electrolytes: electrolyte 1 for devices A based on Br^-/Br_3^- containing 0.9 M DMBIBr, 0.08 M Br_2 and 0.5 M TBP in dry CH_3CN; electrolyte 2 for devices B also based on Br^-/Br_3^- containing 0.9 M DMBIBr, 0.8 M LiBr, 0.08 M Br_2, and 0.5 M TBP in dry CH_3CN; and electrolyte 3 for devices C based on I^-/I_3^- containing 0.6 M DMPII, 0.06 M LiI, 0.04 M I_2, and 0.4 M TBP in dry CH_3CN.

of electrolyte and the Fermi level of TiO_2, but also the suppressed electron recombination.

For a DSC, the collection yield of injected electrons depends on the effective electron-diffusion length (L_n). The longer L_n results in better collection yield of injected electrons. Upon replacement of I^-/I_3^- with Br^-/Br_3^-, the L_n of

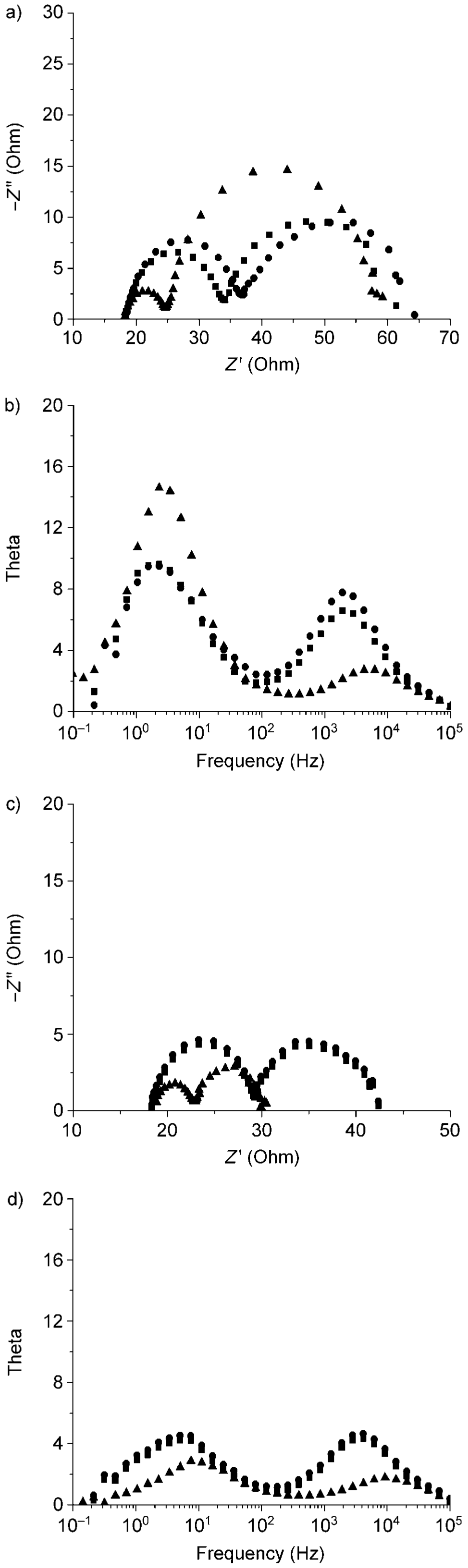

Figure 8. Electrochemical impedance spectra, scanned from 10^{-1} to 10^5 Hz at RT, for devices A (■), B (●), and C (▲), respectively. a, b) Nyquist plots and Bode phase plots for **TC308**-based DSC; c, d) Nyquist plots and Bode phase plots for **TC310**-based DSC. The cells were measured at −0.7 V in the dark. The alternating current (AC) amplitude was set at 10 mV. Devices A are based on 0.9 M DMBIBr, 0.08 M Br_2, and 0.5 M TBP electrolyte in dry CH_3CN; devices B are based on 0.9 M DMBIBr, 0.8 M LiBr, 0.08 M Br_2, and 0.5 M TBP electrolyte in dry CH_3CN; and devices C are based on 0.6 M DMPII, 0.06 M LiI, 0.04 M I_2, and 0.4 M TBP electrolyte in dry CH_3CN.

Table 4. The detailed parameters extracted from electrochemical impedance spectra of DSC based on **TC308** and **TC310** and different electrolytes.

Dye	Device[a]	τ [ms][b]	R_{ct} [ohm cm^{-2}][c]	R_t [ohm cm^{-2}][d]	L_n [μm][e]
TC308	A	78	34	28	18
	B	73	37	29	18
	C	57	25	33	12
TC310	A	38	25	12	23
	B	35	29	13	24
	C	16	23	7	29

[a] Devices A are based on 0.9 M DMBIBr, 0.08 M Br_2, and 0.5 M TBP electrolyte in dry CH_3CN; devices B are based on 0.9 M DMBIBr, 0.8 M LiBr, 0.08 M Br_2, and 0.5 M TBP electrolyte in dry CH_3CN; and devices C are based on 0.6 M DMPII, 0.06 M LiI, 0.04 M I_2, and 0.4 M TBP electrolyte in dry CH_3CN. [b] The electron lifetime (τ) is expressed for electron recombination in TiO_2 films and can be extracted from the angular frequency (ω_{min}) at the midfrequency peak in the Bode phase plot by using $\tau = 1/\omega_{min}$.[20] [c] R_{ct} represents the charge-transfer resistance at the dye/TiO_2/electrolyte interface related to electron recombination. [d] R_t represents the electron-transport resistance in TiO_2 film. [e] The effective electron-diffusion length (L_n) in TiO_2 films reflects the competition between charge collection and recombination: $L_n = L(R_{ct}/R_t)^{1/2}$ (in which L is the thickness of TiO_2 film).[21]

devices A and B became longer than that of devices C for the DSC sensitized by **TC308**, thus a better collection yield of injected electrons was obtained. However, for the DSC sensitized by **TC310**, the L_n became shorter, which accounts for the reduced collection yield of injected electrons obtained upon replacement of I^-/I_3^- with Br^-/Br_3^-. This is one of main reasons why distinctive efficiencies were had for DSCs sensitized by **TC308** and **TC310** upon replacement of Br^-/Br_3^- with I^-/I_3^-.

Dye regeneration: The solar-energy-conversion efficiency of a DSC is strongly dependent on the kinetic competition between electron backtransfer from the conduction band of TiO_2 to the oxidized state of the dye (S^+) and the interception of S^+ by the redox mediator in electrolyte, and is directly proportional to the dye-regeneration yield Φ_r, as shown in Equation (1):

$$\Phi_r = k_r/(k_r + k_b) \tag{1}$$

in which k_r and k_b are rate constants of dye regeneration that occurs in the presence of redox mediator and electron backtransfer that takes place between S^+ and the conduction-band electron, respectively.[22]

The different energy gaps between the HOMO levels of the dyes and the redox potential of electrolytes can lead to different driving forces, and thus different Φ_r. To scrutinize the different Φ_r that occurs in the presence of different electrolytes, nanosecond laser transient-absorbance measurements of TiO_2 films sensitized by **TC308** and **TC310** were performed. The time evolutions of the transient absorbance are shown in Figure 9. The signals over wavelength ranges that extend from 380 to 500 nm and from 430 to 700 nm are assigned to the absorbance of the oxidized form of **TC308** (**TC308**$^+$) and **TC310** (**TC310**$^+$), respectively. The decay of the transient-absorption signal of **TC308**$^+$ and **TC310**$^+$ were recorded at 450 and 600 nm, respectively (Figure 10), and the related data are collected in Table 5.

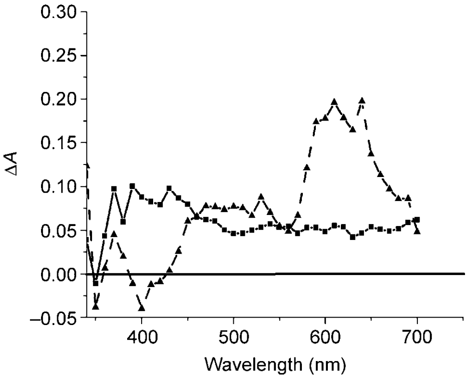

Figure 9. Time-resolved transient-absorption spectra of **TC308** (■) and **TC310** (▲) on TiO_2 films excited at 355 nm.

The kinetics of **TC308**$^+$ transient-absorbance decay exhibited a typical half-lifetime of $\tau_{1/2} = 92.3$ μs. In the presence of electrolytes, the decays of **TC308**$^+$ were all significantly ac-

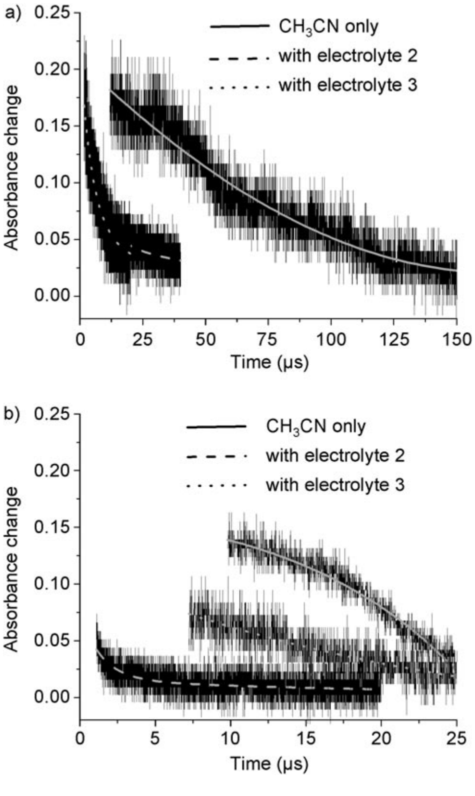

Figure 10. Transient-absorbance decay kinetics of the oxidized form of a) **TC308** and b) **TC310** adsorbed on a mesoporous TiO_2 film in different electrolytes. Electrolyte 2 is based on the Br^-/Br_3^- couple, and electrolyte 3 is based on the I^-/I_3^- couple. The dyes were adsorbed from solutions in CH_2Cl_2. Absorbance changes were measured at a probe wavelength of 450 nm for **TC308** and 600 nm for **TC310** and employed 355 nm laser excitation. The continuous lines drawn on top of the experimental data are single-exponential fit curves.

Table 5. The lifetimes and the rate constants extracted from transient-absorbance measurements of **TC308** and **TC310** absorbed TiO_2 films in different electrolytes.

Dye	Electrolyte	$\tau_{1/2}$ [μs]	k [$\times 10^5$ s^{-1}]
TC308	CH_3CN only	92.3	0.11
	electrolyte 2[a]	6.4	1.56
	electrolyte 3[b]	6.8	1.48
TC310	CH_3CN only	39.8	0.25
	electrolyte 2[a]	23.4	0.43
	electrolyte 3[b]	6.7	1.50

[a] Electrolyte 2 is based on a Br^-/Br_3^- couple. [b] Electrolyte 3 is based on an I^-/I_3^- couple.

celerated with $\tau_{1/2}=6.4$ μs for electrolyte that contained Br^-/Br_3^- and $\tau_{1/2}=6.8$ μs for I^-/I_3^-, respectively. Remarkably, the dye-regeneration kinetics can be described by approximate single-exponential decays with rate constant $k_r=1.56\times10^5$ s^{-1} for electrolyte that contains Br^-/Br_3^- and $k_r=1.48\times10^5$ s^{-1} for I^-/I_3^-, respectively. The data for the electron backtransfer kinetics could also be fitted approximately with a single-exponential decay, a rate constant of $k_b=1.1\times10^4$ s^{-1}, thus leading to Φ_r of 93.4% for electrolyte that contained Br^-/Br_3^- and 93.1% for I^-/I_3^-, respectively. This result reveals that **TC308** can be regenerated efficiently by both Br^-/Br_3^- and I^-/I_3^-. On the other hand, the Φ_r of **TC310** are determined to be 63.2% for electrolyte that contains Br^-/Br_3^- and 85.7% for I^-/I_3^-, respectively. This means that **TC310** can only be regenerated efficiently by I^-/I_3^- and not by Br^-/Br_3^-. The HOMO level of **TC308** is 1.43 V, which is much more positive than both $E(Br^-/Br_3^-)$ and $E(I^-/I_3^-)$, thus the driving forces of dye regeneration are sufficient with both Br^-/Br_3^- and I^-/I_3^-. However, the HOMO level of **TC310** is more positive than $E(I^-/I_3^-)$ but similar to $E(Br^-/Br_3^-)$, thus the driving force of the reduction of **TC310**$^+$ is only sufficient with I^-/I_3^- and insufficient with Br^-/Br_3^-.

Conclusion

We have synthesized a series of novel metal-free organic dyes **TC301–TC310** with relatively high HOMO levels for application in DSCs based on electrolytes that contain Br^-/Br_3^- and I^-/I_3^-. Our purposes for the dye design are summarized by two major points: 1) to study the Li^+-ion effects on the photoelectrochemical properties of the dyes and the performance of the DSC, and 2) to scrutinize the relationship between the HOMO levels of the dyes and the performance of the DSC based on electrolytes that contain Br^-/Br_3^- and I^-/I_3^-. The addition of Li^+ ions in electrolytes can broaden the absorption spectra of the dyes on TiO_2 films and shift the LUMO levels of the dyes and the conduction band of TiO_2 towards positive positions, thereby leading to the increase in J_{sc} and the decrease in V_{oc}. Upon using Br^-/Br_3^- instead of I^-/I_3^-, a large increase of V_{oc} is attributed to not only the enlarged energy gap between the redox potential of electrolyte and the Fermi level of TiO_2, but also the suppressed electron recombination. Electrochemical impedance spectra studies reveal that the effective electron-diffusion lengths (L_n) become longer upon using Br^-/Br_3^- instead of I^-/I_3^- for the dyes for which the HOMO levels are more positive than the redox potential of Br^-/Br_3^-, but become shorter for the dyes for which the HOMO levels are similar to the redox potential of Br^-/Br_3^-. IPCE action spectra and nanosecond laser transient-absorption study reveal that the dye-regeneration yields (Φ_r) depend on the potential difference between the HOMO levels of the dyes and the redox couple of Br^-/Br_3^-.

Experimental Section

Analytical methods and measurements: Absorption and emission spectra were recorded in a quartz cell with 1 cm path length using Agilent HP 8453 (USA) and Photon Technology International 700 (USA) spectrophotometers, respectively. ^{1}H NMR spectra were measured using a Varian INOVA 400 MHz (USA) with the chemical shifts measured against TMS. MS data were obtained using GCT CA156 (UK), HP1100 LC/MSD (USA), and LC/Q-TOF MS (UK) instruments. Electrochemical redox potentials were obtained by cyclic voltammetry (CV) using a three-electrode cell and an electrochemistry workstation (BAS100B, USA). The working electrode was a glass carbon disc electrode; the auxiliary electrode was a Pt wire, and Ag/Ag^+ was used as reference electrode. Tetrabutylammonium hexaflourophosphate ($TBAPF_6$, 0.1 M) was used as supporting electrolyte in DMF. Ferrocene was added to each sample solution at the end of the experiments and the ferrocenium/ferrocene (Fc/Fc^+) redox couple was used as an internal potential reference. The potentials versus NHE were calibrated by the addition of 630 mV to the potentials versus Fc/Fc^+.[11] Electrochemical impedance spectroscopy (EIS) for DSC in the dark with bias of −0.7 V was measured using an impedance/gain-phase analyzer (PARSTAT 2273, USA). The spectra were scanned in a frequency range of 10^{-1}–10^5 Hz at RT. The alternating current (AC) amplitude was set at 10 mV. Transient-absorption measurements were carried out using a nanosecond-laser flash photolysis setup (LP920, Edinburgh Instrument Ltd., UK). Excitation pulses at 355 nm (1.1 mJ, 7 ns full width at half-maximum) were obtained using a Quanta-Ray master optical parametric oscillator (MOPO) pumped by a Quanta-Ray 230 Nd:YAG laser (355 nm). The probe light was provided by a 75WXe arc lamp and was collinear with the excitation beam. After passing through the sample, the probe light was spectrally filtered with two monochromators and finally detected using a Hamamatsu R928 photomultiplier tube. Individual trace kinetics were analyzed using the deconvolution software Spectra Solve.[23]

DSC fabrication: A layer of approximately 2 μm TiO_2 (13 nm paste, DHS-TPP3, Heptachroma, China) was coated on the F-doped tin oxide conducting glass (TEC15, 15 Ω per square, Pilkington, USA) by screen printing and then dried for 6 min at 125 °C. This procedure was repeated 6 times (around 12 μm) and finally coated by a layer (around 4 μm) of TiO_2 paste (DHS-SLP1, Heptachroma, China) as scattering layer. The double-layer TiO_2 electrodes (area: 6×6 mm) were gradually heated under an air flow at 325 °C for 5 min, at 375 °C for 5 min, at 450 °C for 15 min, and at 500 °C for 15 min. The sintered film was further treated with 40 mM $TiCl_4$ aqueous solution at 70 °C for 30 min, then washed with ethanol and water, and annealed at 500 °C for 30 min. After the film was cooled to 40 °C, it was immersed into a 2×10^{-4} M dye bath in CH_2Cl_2 solution and maintained in the dark for 8 h. The electrode was then rinsed with CH_2Cl_2 and dried. The hermetically sealed cells were fabricated by assembling the dye-loaded film as the working electrode and Pt-coated conducting glass as the counterelectrode separated with a hot-melt Surlyn 1702 film (25 μm, Dupont). The electrolyte was introduced into the cell by means of vacuum backfilling from a hole in the back of the counterelectrode. Finally, the hole was also sealed using Surlyn 1702 film and cover glass.

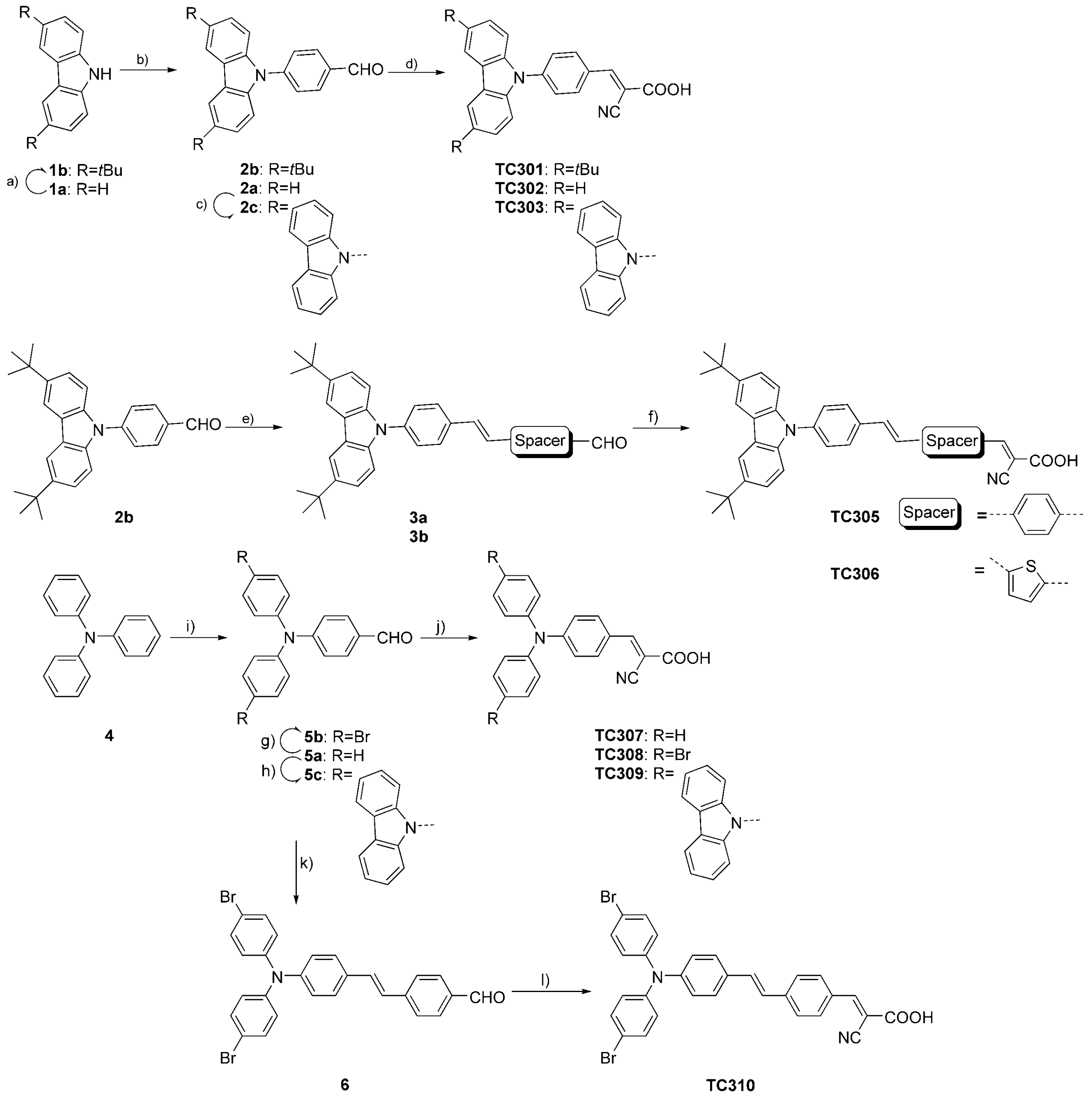

Scheme 2. Synthetic routes of the dyes **TC301**–**TC310**. a) compound **1a**, *t*BuCl, RT, 24 h; b) 4-bromobenzaldehyde, Pd(OAc)$_2$, *t*Bu$_3$P, toluene, reflux, 24 h; c) KI, KIO$_3$, CH$_3$COOH, 80 °C, 4 h; d) cyanoacetic acid, piperidine, CH$_3$CN, reflux, 3 h; e) 1) NaBH$_4$, CH$_2$Cl$_2$, C$_2$H$_5$OH, RT, 2 h; 2) PPh$_3$·HBr, CHCl$_3$, reflux, 2 h; 3) terephthalaldehyde or thiophene-2,5-dicarbaldehyde, [18]crown-6, K$_2$CO$_3$, DMF, RT, 2 h; 4) I$_2$, THF, reflux, 8 h; f) cyanoacetic acid, piperidine, CH$_3$CN, reflux, 3 h; g) Br$_2$, CHCl$_3$, ice–water, 3 h; h) KI, KIO$_3$, CH$_3$COOH, 80 °C, 4 h; p) compound **1a**, Pd(OAc)$_2$, *t*Bu$_3$P, toluene, reflux, 24 h; i) POCl$_3$, DMF, ClCH$_2$CH$_2$Cl, reflux, 6 h; j) cyanoacetic acid, piperidine, CH$_3$CN, reflux, 3 h; k) 1) NaBH$_4$, CH$_2$Cl$_2$, C$_2$H$_5$OH, RT, 2 h; 2) PPh$_3$·HBr, CHCl$_3$, reflux, 2 h; 3) terephthalaldehyde, [18]crown-6, K$_2$CO$_3$, DMF, RT, 2 h; 4) I$_2$, THF, reflux, 8 h; and l) cyanoacetic acid, piperidine, CH$_3$CN, reflux, 3 h.

Photovoltaic properties measurements: The irradiation source for the photocurrent–voltage (*J*–*V*) measurement was an AM 1.5 solar simulator (16S-002, SolarLight Co. Ltd., USA). The incident light intensity was 100 mW cm^{-2} calibrated with a standard Si solar cell. The tested solar cells were masked to a working area of 0.159 cm^2. The current–voltage curves were obtained by the linear-sweep voltammetry (LSV) method using an electrochemical workstation (LK9805, Lanlike Co. Ltd., China). The measurement of the incident photon-to-current conversion efficiency (IPCE) was performed using a Hypermonolight (SM-25, Jasco Co. Ltd., Japan).

Preparation of the sample for laser-flash measurements: The transparent TiO$_2$ film (approximately 3 mm thick) was prepared from a commercial TiO$_2$ paste (DHS-TPP3, Heptachroma, China) by a doctor-blading method and sintering at 500 °C for 30 min in air. After the film was cooled to RT, it was immersed in a 2×10^{-4} M dye solution in CH$_2$Cl$_2$ and kept in darkness for 5 min. The TiO$_2$ films with anchoring dyes were cut into the same size (2.5 cm × 1.3 cm) for laser-flash measurements.

Synthesis: The synthetic routes of the dyes **TC301**–**TC310** are shown in Scheme 2, and the detailed synthetic procedures are described in Supporting Information.

Acknowledgements

We gratefully acknowledge the financial support of this work from the following sources: China Natural Science Foundation (grant no. 20633020), the National Basic Research Program of China (grant no. 2009CB220009), the Ministry of Science and Technology (MOST) (grant no. 2001CCA02500), the Ministry of Education (MOE), the Program for Changjiang Scholars and Innovation Research Team in university (PCSIRT), the Swedish Energy Agency, the Swedish Research Council, and the K&A Wallenberg Foundation. The authors are grateful to Professor Can Li, Dr. Jingying Shi, and Min Zhong at the Dalian Institute of Chemical Physics, CAS, China, for EIS measurement and helpful discussions.

---

[1] a) B. O'Regan, M. Grätzel, *Nature* **1991**, *353*, 737; b) A. Hagfeldt, M. Grätzel, *Acc. Chem. Res.* **2000**, *33*, 269.

[2] a) M. Grätzel, *Pure Appl. Chem.* **2001**, *73*, 459; b) C. Nasr, S. Hotchandani, P. V. Kamat, *J. Phys. Chem. B* **1998**, *102*, 4944.

[3] A. Hagfeldt, M. Grätzel, *Chem. Rev.* **1995**, *95*, 49.

[4] M. Grätzel, *J. Photochem. Photobiol. A* **2004**, *164*, 3.

[5] a) B. A. Gregg, F. Pichot, S. Ferrere, C. R. Fields, *J. Phys. Chem. B* **2001**, *105*, 1422; b) B. A. Gregg, *Coord. Chem. Rev.* **2004**, *248*, 1215.

[6] a) H. Nusbaumer, J.-E. Moser, S. M. Zakeeruddin, M. K. Nazeeruddin, M. Grätzel, *J. Phys. Chem. B* **2001**, *105*, 10461; b) H. Nusbaumer, S. M. Zakeeruddin, J.-E. Moser, M. Grätzel, *Chem. Eur. J.* **2003**, *9*, 3756; c) S. A. Sapp, C. M. Elliott, C. Contado, S. Caramori, C. A. Bignozzi, *J. Am. Chem. Soc.* **2002**, *124*, 11215.

[7] Z. Zhang, P. Chen, T. N. Murakami, S. M. Zakeeruddin, M. Grätzel, *Adv. Funct. Mater.* **2008**, *18*, 341.

[8] a) S. Ito, P. Chen, P. Comte, M. K. Nazeeruddin, P. Liska, P. Péchy, M. Grätzel, *Prog. Photovoltaics* **2007**, *15*, 603; b) G. Redmond, D. Fitzmaurice, *J. Phys. Chem.* **1993**, *97*, 1426.

[9] Z. Wang, K. Sayama, H. Sugihara, *J. Phys. Chem. B* **2005**, *109*, 22449.

[10] C. Teng, X. Yang, C. Yuan, C. Li, R. Chen, H. Tian, S. Li, A. Hagfeldt, L. Sun, *Org. Lett.* **2009**, *11*, 5542.

[11] P. V. Kamat, *Chem. Rev.* **1993**, *93*, 267.

[12] C. Reichardt, *Chem. Rev.* **1994**, *94*, 2319.

[13] S. Roquet, A. Cravino, P. Leriche, O. Alévêque, P. Frère, J. Roncali, *J. Am. Chem. Soc.* **2006**, *128*, 3459.

[14] K. Hara, T. Sato, R. Katoh, A. Furube, T. Yoshihara, M. Murai, M. Kurashige, S. Ito, A. Shinpo, S. Suga, H. Arakawa, *Adv. Funct. Mater.* **2005**, *15*, 246.

[15] A. Furube, R. Katoh, K. Hara, T. Sato, S. Murata, H. Arakawa, M. Tachiya, *J. Phys. Chem. B* **2005**, *109*, 16406.

[16] D. P. Hagberg, T. Edvinsson, T. Marinado, G. Boschloo, A. Hagfeldt, L. Sun, *Chem. Commun.* **2006**, *2245*.

[17] a) Gaussian 03, Revision C.02, M. J. Frisch, G. W. Trucks, H. B. Schlegel, G. E. Scuseria, M. A. Robb, J. R. Cheeseman, J. A. Montgomery, Jr., T. Vreven, K. N. Kudin, J. C. Burant, J. M. Millam, S. S. Iyengar, J. Tomasi, V. Barone, B. Mennucci, M. Cossi, G. Scalmani, N. Rega, G. A. Petersson, H. Nakatsuji, M. Hada, M. Ehara, K. Toyota, R. Fukuda, J. Hasegawa, M. Ishida, T. Nakajima, Y. Honda, O. Kitao, H. Nakai, M. Klene, X. Li, J. E. Knox, H. P. Hratchian, J. B. Cross, V. Bakken, C. Adamo, J. Jaramillo, R. Gomperts, R. E. Stratmann, O. Yazyev, A. J. Austin, R. Cammi, C. Pomelli, J. W. Ochterski, P. Y. Ayala, K. Morokuma, G. A. Voth, P. Salvador, J. J. Dannenberg, V. G. Zakrzewski, S. Dapprich, A. D. Daniels, M. C. Strain, O. Farkas, D. K. Malick, A. D. Rabuck, K. Raghavachari, J. B. Foresman, J. V. Ortiz, Q. Cui, A. G. Baboul, S. Clifford, J. Cioslowski, B. B. Stefanov, G. Liu, A. Liashenko, P. Piskorz, I. Komaromi, R. L. Martin, D. J. Fox, T. Keith, M. A. Al-Laham, C. Y. Peng, A. Nanayakkara, M. Challacombe, P. M. W. Gill, B. Johnson, W. Chen, M. W. Wong, C. Gonzalez, J. A. Pople, Gaussian, Inc.: Wallingford, CT, **2004**; b) A. D. Becke, *J. Chem. Phys.* **1993**, *98*, 5648; c) R. Ditchfield, W. J. Herhe, J. A. Pople, *J. Chem. Phys.* **1971**, *54*, 724.

[18] G. Redmond, D. Fitzmaurice, *J. Phys. Chem.* **1993**, *97*, 1426.

[19] G. Oskam, B. V. Bergeron, G. J. Meyer, P. C. Searson, *J. Phys. Chem. B* **2001**, *105*, 6867.

[20] R. Kern, R. Sastrawan, J. Ferber, R. Stangl, J. Luther, *Electrochim. Acta* **2002**, *47*, 4213.

[21] F. Fabregat-Santiago, J. Bisquert, L. Cevey, P. Chen, M. Wang, S. M. Zakeeruddin, M. Grätzel, *J. Am. Chem. Soc.* **2009**, *131*, 558.

[22] D. Kuang, S. Ito, B. Wenger, C. Klein, J. Moser, R. Humphry-Baker, S. M. Zakeeruddin, M. Grätzel, *J. Am. Chem. Soc.* **2006**, *128*, 4146.

[23] Spectra Solve 2.01, Lastek Pty. Ltd., **1997**.

Received: February 22, 2010